https://doi.org/10.2352/issn.2169-2629.2019.27.30
Reprinted from
Journal of Imaging Science and Technology® 63(4): 040407-1–040407-11, 2019.

Angular Color Prediction Model for Anisotropic Halftone Prints on a Metallic Substrate

P. Pjanic
Ecole Polytechnique Fédérale de Lausane (EPFL), Switzerland

L. Yang and A. Teleman
RISE, Stockholm, Sweden

R. D. Hersch▲
Ecole Polytechnique Fédérale de Lausane (EPFL), Switzerland
E-mail: rd.hersch@epfl.ch

Abstract. *Under specular reflection, non-isotropic halftones such as line halftones printed on an ink-receiving plastic layer superposed with a metallic layer change their colors upon in-plane rotation of the print. This color change is due to the orientation-dependent optical dot gain of the halftone. A strong dot gain occurs when the incident light is perpendicular to the halftone line structure. A color prediction model is proposed which predicts under specular reflection the color of cyan, magenta and yellow line halftones as a function of the azimuthal rotation angle, the incident angle and the line frequency. The model is calibrated by measuring 17 reflectances at the (25° : 25°) measurement geometry, with the incident light parallel to the halftone lines. The model has been tested for several azimuthal rotation and incident viewing angles, each time for 125 different cyan, magenta and yellow ink surface coverages. The obtained prediction accuracies are between* $\Delta E_{94} = 3.5$ *and* $\Delta E_{94} = 7$.

[DOI: 10.2352/J.ImagingSci.Technol.2019.63.4.040407]

1. INTRODUCTION

Non-isotropic halftones such as line halftones printed on a metallic substrate may change their colors upon in-plane rotation. The color is changed due to the *direction-dependent optical dot gain*. We present a model that predicts the color of line halftone prints by relying on the interaction between the incident light and the print medium. This model predicts reflectances in function of the azimuthal rotation angle, the specular incident angle and the line frequency. This spectral prediction model was established based on the cross-section micrographs taken with a scanning electron microscope (SEM). The cross-section micrographs revealed the thickness of the ink attracting transparent polymer on top of the metallic layer (see Figure 1). This transparent ink-receiving layer elevates the ink halftone with respect to the specularly reflecting metallic layer. Due to this elevation, the effective area affected by the ink halftone is increased and the area that reflects the bare metal is reduced (Figure 2) when viewed in transverse direction. The resulting anisotropic ink dot gain reinforces the colorfulness of halftones in halftone lines perpendicular to the incident light.

The approach taken to create the viewing angle and azimuthal rotation-dependent spectral prediction model predicting colors under specular viewing conditions relies on the following concepts:

- Determination of the different halftone areas traversed by the light rays reaching the eye,
- Determination of the ink transmittances under specular reflection,
- Determination of the halftone line positions according to the incident light ray angle and to the azimuthal orientation of the line halftone,
- Determination of the colorant areas associated with each combination of incident rays and specularly reflected rays, and
- Neugebauer-type summation of the contributions of the spectral light attenuations from all possible incident and exiting ray ink area combinations.

In order to be used in real applications, the present color prediction model needs to evolve toward an interactive software framework offering color proofing capabilities on displays. Such a framework would then offer new capabilities for artistic design, advertisement and document security.

2. RELATED WORK

Hersch et al. created a security feature by combining a silver ink and conventional inks to print on paper color images with metallic color patterns that are hidden under non-specular viewing conditions and revealed under specular viewing conditions [1].

Matusik et al. extended classic color reproduction with the aim of reproducing also the BRDF (bidirectional reflectance distribution function) of a flat original [2]. They used a blend of conventional inks and of glossy metallic inks with specific BRDFs and reproduced the

▲ IS&T Member.

Received Mar. 18, 2019; accepted for publication June 16, 2019; published online Aug. 22, 2019. Associate Editor: Michael Murdoch.

1062-3701/2019/63(4)/040407/11/$25.00

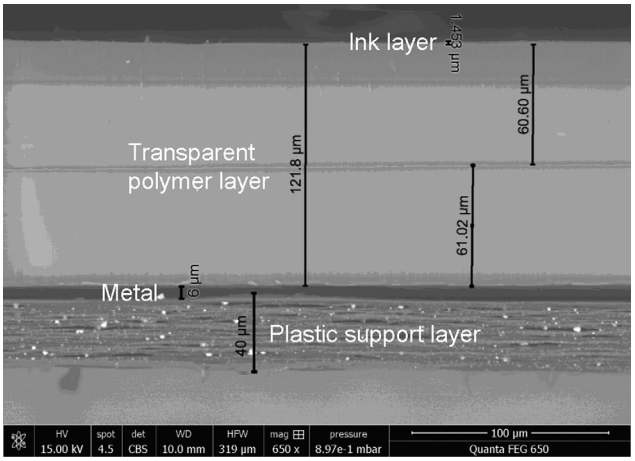

Figure 1. Photograph taken with a scanning electron microscope.

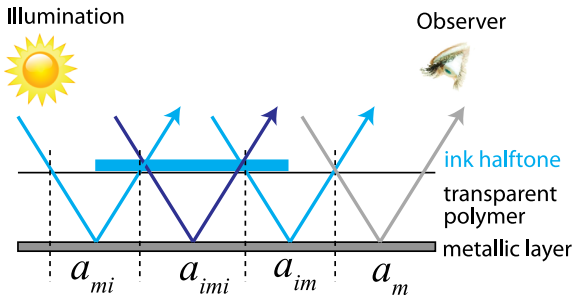

Figure 2. Light propagation through the halftoned metallic print. The light gray arrow shows the reduced size area where light is reflected from the bare metal, without traversing any ink layer.

original by an extended halftoning process. Malzbender et al. used halftoning on top of an array of specularly reflecting spherical depressions to create images with desired reflection functions [3].

Babaei and Hersch applied the Yule–Nielsen spectral prediction model for predicting the colors reflected by metallic halftones formed with metallic inks such as metallic cyan, metallic magenta, gold and silver [4]. By calibrating the model separately at each illumination and viewing condition, they obtained good prediction accuracies. They also proposed strategies for performing the color separation with the goal of optimizing print properties such as gamut size, color constancy, halftone visibility and image graininess [5].

Pjanic and Hersch created a color reproduction workflow for printing with conventional inks on a metallic substrate [6]. In order to establish the correspondence between amounts of inks and resulting color under specular reflection, they used a cellular Yule–Nielsen spectral prediction model. This model is calibrated with patch reflectances measured under specular reflection. The halftones are printed with classical mutually rotated dot screens to limit the amount of color deviations that may occur upon rotation or tilting of the prints.

In a further work, by printing on a metallic substrate with an optimal amount of white and of cyan, magenta and yellow inks, Pjanic and Hersch created prints that are partly specularly and partly diffusely reflecting [7]. By relying on the trade-off between amounts of the light diffusing white ink and amounts of cyan, magenta and yellow inks to control lightness, these prints enable hiding patterns such as text or graphical symbols in one viewing mode, specular or non-specular, and reveal them in the other viewing mode.

Pjanic and Hersch [8] also proposed a color reproduction framework for creating specularly reflecting color images printed on a metallic substrate that changes hue or chroma upon in-plane rotation by 90°. This framework is based on the anisotropic dot gain of line halftones when viewed under specular reflection. It relies on a Yule–Nielsen-type spectral prediction model predicting the color of either the non-rotated or the 90° in-plane rotated cross-halftones formed of superpositions of horizontal and vertical cyan, magenta and yellow line halftones. In contrast to the present paper, that prediction model predicts colors only for a single incident angle (25°) and at two azimuthal orientations of the print halftone, perpendicular to the incident light and parallel to the incident light.

In the present work, by relying on a physical approach, the authors propose to predict the colors of line halftones printed on metal at any azimuthal rotation angle and for any incident angle with respect to the print normal.

3. CROSS-SECTION OF THE METALLIC SHEET

The orientation-dependent dot gain depends on the distance between the ink layer and the specularly reflecting substrate. To obtain this distance, we decided to perform measurements with a scanning electron microscope. We analyzed the structure of the halftone printed on the metallic sheet. We determined the composition of the print medium as well as the thicknesses of the individual layers.

For acquiring and analyzing the microscope images, the setup comprised the following items: an FEI scanning electron microscope Qanta FEG 650 (field emission gun) equipped with a concentric backscattered electron detector, an X-Max silicon detector, an energy dispersive spectrometer and the AZtec image analysis software from Oxford Instruments. The working conditions were as follows: in low vacuum mode, the pressure in the sample chamber was about 0.6 mbar, the accelerating voltage 15 kV and the working distance 10 mm. The magnification used for the cross-section was 650×. No conductive coating was used for the analyzed samples. The cross-section was made manually by means of a razor blade.

Fig. 1 shows the photograph of the cross-section obtained with the scanning electron microscope. We deduced that the metallic print has four main components. From bottom to top, they are: (a) the plastic support layer at the bottom, (b) the metallic layer, (c) the ink-receiving transparent polymer and (d) the ink halftone layer.

We observed that the thicknesses are the following:

- Plastic support layer: 40 µm,
- The metallic layer: 6 µm,

- Ink-receiving polymer layer: 120 μm,
- Ink layer : 1.4 μm.

Furthermore, we see that the transparent polymer is divided into several sub-layers.

4. MODELING THE LIGHT PATHS THROUGH THE METALLIC PRINT MEDIA

In order to establish a model predicting the color observable under specular reflection, it is important to describe how light interacts with the metallic print, accounting for the layers that appear in the cross-section micrographs. We assume that the metallic halftone is observed under specular reflection and that all printed color inks are transparent. We shall freely choose the incident angle, the azimuthal orientation of the print and the line screen frequency.

Fig. 2 shows several cases of how the incoming light interacts with the metallic halftone print. The first case is where the incoming light traverses the ink layer, bounces off the metallic surface, passes through the ink layer again and then reaches the observer (a_{imi}). The second case is where the light directly reaches the metallic surface, is specularly reflected and traverses the ink layer before reaching the observer (a_{mi}). In the third case, the incoming light traverses the ink layer, bounces off the metallic surface and then reaches the observer (a_{im}). Finally, the fourth case is where the incoming light is reflected off the metallic surface without traversing the ink layer (a_m).

The sizes of the a_{imi}, a_{mi}, a_{im} and a_m areas depend on the incident angle θ, the azimuthal rotation angle φ of the print, the halftone shape and the screen frequency. For example, if the halftone shape is round, the azimuthal rotation (φ) does not modify the a_{imi}, a_{mi}, a_{im} and a_m areas. On the contrary, when the halftone is a line screen, the a_{imi}, a_{mi}, a_{im} and a_m areas create upon azimuthal rotation a strong color change due to the change in dot gain. In the present paper, we consider only line halftones.

First, we deduce the reflectances of the a_{imi}, a_{mi}, a_{im} and a_m areas. Then, we estimate the overall reflectance of the line halftone $R(\lambda)$. To simplify the prediction model, we assume that there are no multiple reflections occurring between the metallic layer and the polymer–air interface. Furthermore, we assume that we can measure the reflectance of the metal layer $R_{Metal}(\lambda)$ and estimate the transmittance of the printed ink $T_{Ink}(\lambda)$ by using the measured reflectance of the fulltone ink (Eq. (8)) under specular reflection.

Once the surface coverages of the a_{imi}, a_{mi}, a_{im} and a_m areas are known, we can assume that the spectral Neugebauer equations [9] are valid when viewing the print under specular reflection. We also assume that the amount of the diffusely reflected light is small. The overall reflectance $R(\lambda)$ of the line halftone can then be predicted

$$R(\lambda) = a_{imi} T_{Ink}^2(\lambda) R_{Metal}(\lambda) + a_{mi} T_{Ink}(\lambda) R_{Metal}(\lambda) + a_{im} T_{Ink}(\lambda) R_{Metal}(\lambda) + a_m R_{Metal}(\lambda) \quad (1)$$

where a_{imi} is the area where the light travels twice through the ink layer, a_{mi} is the area where the light is reflected off the metallic surface and travels once through the ink layer, a_{im} is the area where the light travels through the ink layer, hits the metal and is then reflected to the observer and a_m is the area where the light hits only the metallic surface. $T_{Ink}(\lambda)$ is the transmittance of the ink layer and $R_{Metal}(\lambda)$ is the reflectance of the unprinted coated metallic sheet.

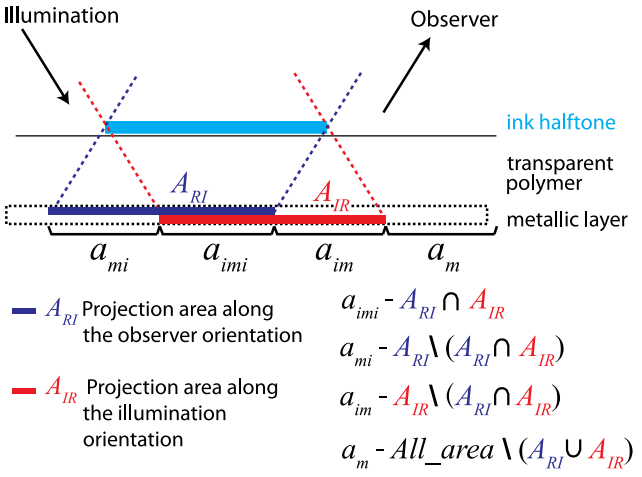

Figure 3. The calculation of the ar_{imi}, a_{mi}, a_{im} and a_m areas based on the A_{RI} and A_{IR} projected ink areas.

5. SINGLE COLORANT SPECTRAL PREDICTION MODEL

To deduce the a_{imi}, a_{mi}, a_{im} and a_m areas, we have to account for the incident angle θ, the azimuthal angle φ, the line screen frequency and the surface coverage of the ink. The model presented in the present section is valid only for lines that are formed by a single colorant. The extension of the model to line-on-line multi-ink line halftones is presented in Section 6.

Let us calculate the a_{imi}, a_{mi}, a_{im} and a_m areas. In order to simplify the model, we assume that the specularly reflected light rays are collimated. This is the case when the observer is sufficiently far away from the print and/or the print is relatively small in size.

The first step is to deduce the A_{RI} and A_{IR} areas that correspond to the projections of the inked area onto the metallic base, according to the illumination and observer orientations (see Figure 3). These areas depend on the incident angle θ and on the azimuthal rotation angle φ. The intersection of these two projection areas yields the area a_{imi}, where light traverses twice the ink layer. Area a_m is the surface not covered by either of the two projections. Area a_{mi} is obtained by excluding the a_{imi} area from the A_{RI} area and area a_{im} is obtained by excluding the a_{imi} area from the A_{IR} area (see Fig. 3).

5.1 *Accounting for the Incident Angle, Azimuthal Angle and Line Frequency*

The areas A_{RI} and A_{IR} of the line halftone are calculated in function of the incident angle θ and the azimuthal rotation angle φ. Based on the input angles (θ,φ) and the thickness d of the transparent polymer layer, we can calculate the lateral

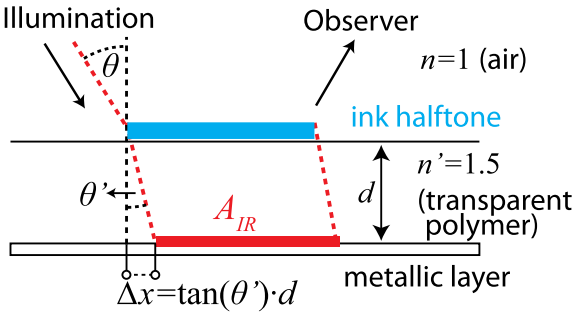

(a) Projection along the illumination direction

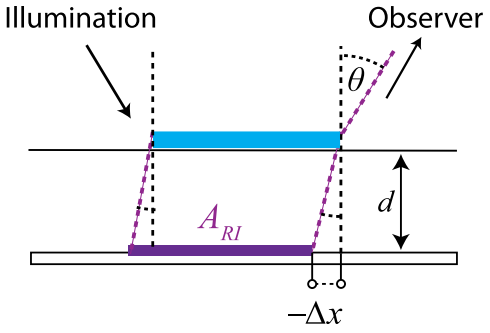

(b) Projection along the observation direction

Figure 4. Calculation of the Δx displacement in function of incident angle θ, of the height of the transparent polymer layer d and of refraction index n'. The refraction angle inside the polymer layer is $\theta' = \arcsin(\sin(\theta)/n')$.

displacement Δx that defines the projections A_{RI} and A_{IR}. Figure 4(a) shows the projected area A_{IR} of the ink surface with lateral displacement Δx. Fig. 4(b) shows the projected area A_{RI} with displacement value $-\Delta x$. According to Snell's law, we account for the refraction of the incident light. We also assume that the refraction index of the transparent polymer is $n = 1.5$.

The lateral displacement Δx of the projections also depends on the azimuthal rotation (φ) of the print. Figure 5a shows that if the halftone lines are perpendicular to the incoming light, i.e., $\varphi = 0°$, the lateral displacement is maximal. However, if the lines are parallel to the incoming light, i.e., $\varphi = 90°$, then the lateral displacement is minimal (Fig. 5b). As shown in Fig. 5c, we account for the azimuthal rotation (φ) of the print by multiplying the maximal displacement with $\cos(\varphi)$.

5.2 *Deducing the Areas Inside a Screen Element Tile*

In order to accurately calculate areas of a_{imi}, a_{mi}, a_{im} and a_m of a screen element tile for any given incident angle θ and azimuthal rotation angle φ, we focus on the cross-section of a line screen element. Figure 6(a) shows that the parallel projection areas A_{RI} and A_{IR} are wrapped within one tile, i.e., part of the parallel projections that are located out of the tile area (L) appears on the other side of the tile (L'). With this wrap-around property, we can correctly calculate the projection areas A_{RI} and A_{IR} that are located inside one screen element, regardless of how large or small the Δx value

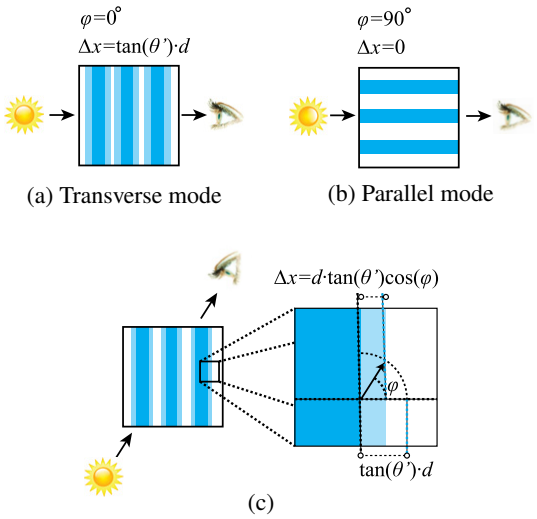

Figure 5. Lateral displacement Δx depending on the azimuthal rotation angle φ: (a) if $\varphi = 0°$, then $\Delta x = \tan(\theta') \cdot d$, (b) if $\varphi = 90°$, then $\Delta x = 0$ and (c) for any φ, the Δx is calculated as $\Delta x = d \tan(\theta') \cdot \cos(\varphi)$.

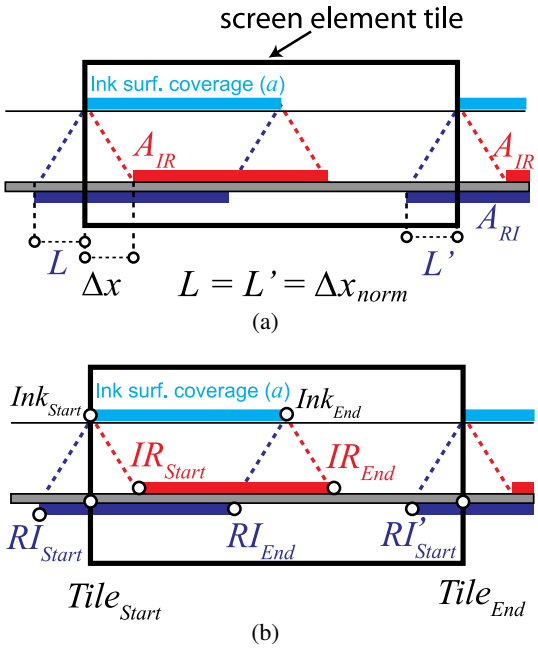

Figure 6. Calculating A_{RI} (blue) and A_{IR} (red) projections located inside one line screen element, according to effective ink surface coverage a and the displacement Δx_{norm}.

is. As the screen element tiles the plane, it is enough to deduce the A_{RI} and the A_{IR} projections for one screen element.

Let us present the algorithm for calculating the areas A_{RI} and A_{IR} inside one screen element in function of the normalized lateral displacement value Δx_{norm}. The Δx_{norm} value is obtained by normalizing the displacement Δx (Fig. 5c) by the distance between $Tile_{Start}$ and $Tile_{End}$ (Fig. 6), representing the width of the line screen element. Then, using the A_{RI} and A_{IR} areas, we calculate the a_{imi}, a_{mi}, a_{im} and

a_m areas (Fig. 3) used in Eq. (1) to calculate the overall reflectance of the sample. Let us describe the algorithm:

- We normalize Δx by the width T of the line halftone element

$$T = \frac{1}{f_l \cdot k}; \quad \Delta x_{\text{norm}} = \frac{\Delta x}{T} \tag{2}$$

where Δx_{norm} is the normalized displacement, f_l is the screen frequency in number of screen lines per inch, $k(= 39.37)$ is the constant giving the number of inches per meter and T is the screen element period in meters.

- Using the displacement value Δx_{norm} and the ink surface coverage a, we calculate the values of IR_{Start}, IR_{End}, RI_{Start} and RI_{End} (see Fig. 6b) as follows:

$$\begin{aligned} IR_{\text{Start}} &= Ink_{\text{Start}} + \Delta x_{\text{norm}}; \quad & IR_{\text{End}} &= Ink_{\text{End}} + \Delta x_{\text{norm}} \\ RI_{\text{Start}} &= Ink_{\text{Start}} - \Delta x_{\text{norm}}; \quad & RI_{\text{End}} &= Ink_{\text{End}} - \Delta x_{\text{norm}} \end{aligned} \tag{3}$$

where Ink_{Start} and Ink_{End} are positions relative to the line screen width.

- Some of the IR_{Start}, IR_{End}, RI_{Start} and RI_{End} points might be located outside the tile area (see RI_{Start} in Fig. 6b). However, due to the wrap-around property of the projections, we can accurately calculate IR'_{Start}, IR'_{End}, RI'_{Start} and RI'_{End} as follows:

$$\begin{aligned} IR'_{\text{Start}} &= IR_{\text{Start}} \bmod 1; \quad & IR'_{\text{End}} &= IR_{\text{End}} \bmod 1; \\ RI'_{\text{Start}} &= RI_{\text{Start}} \bmod 1; \quad & RI'_{\text{End}} &= RI_{\text{End}} \bmod 1 \end{aligned} \tag{4}$$

- We deduce the areas A_{RI} or A_{IR} inside the tile:

$$\begin{aligned} &\text{If } RI'_{\text{End}} < RI'_{\text{Start}} \text{ then} \\ &\quad A_{RI} = [Tile_{\text{Start}}\, RI'_{\text{End}}] \cup [RI'_{\text{Start}}\, Tile_{\text{End}}] \\ &\text{If } RI'_{\text{End}} > RI'_{\text{Start}} \text{ then } A_{RI} = [RI'_{\text{Start}}\, RI'_{\text{End}}] \\ &\text{If } IR'_{\text{End}} < IR'_{\text{Start}} \text{ then} \\ &A_{IR} = [Tile_{\text{Start}}\, IR'_{\text{End}}] \cup [IR'_{\text{Start}}\, Tile_{\text{End}}] \\ &\text{If } IR'_{\text{End}} > IR'_{\text{Start}} \text{ then } A_{IR} = [IR'_{\text{Start}}\, IR'_{\text{End}}] \end{aligned} \tag{5}$$

- Finally, using the A_{RI} and A_{IR} projection areas, we calculate the a_{imi}, a_{mi}, a_{im} and a_m areas (see Fig. 3) as follows:

$$\begin{aligned} a_{imi} &= A_{RI} \cap A_{IR} \\ a_{mi} &= A_{RI} \setminus (A_{RI} \cap A_{IR}) \\ a_{im} &= A_{RI} \setminus (A_{RI} \cap A_{IR}) \\ a_m &= [Tile_{\text{Start}}\, Tile_{\text{End}}] \setminus (A_{RI} \cup A_{IR}). \end{aligned} \tag{6}$$

5.3 *Accounting for the Physical Dot Gain*

An ink dot printed on the metallic substrate can physically spread beyond its nominal boundaries. This effect is called the physical dot gain. Prints with a large physical dot gain are darker and more chromatic than prints with a small physical dot gain. By establishing ink spreading curves, we account for the physical dot gain. Ink spreading curves map nominal ink surface coverages to effective ink surface coverages, i.e., surface coverages of inks that account for the dot gain [10].

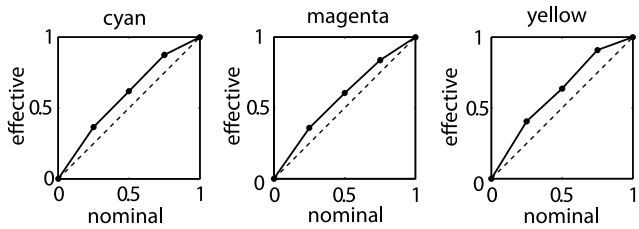

Figure 7. Ink spreading curves accounting for the physical dot gain of the ink on metal, deduced from measurements in parallel mode ($\varphi = 90°$).

When the line halftone is oriented in the parallel mode, we assume that the A_{RI} and A_{IR} projections are exactly at the same place (Fig. 5b, where $\varphi = 90°$, $\Delta x = 0$). In the parallel mode, the incoming light rays hit either only the metallic surface or travel twice through the ink layer. To deduce the effective ink surface coverage in parallel mode, we use Eq. (7) that fits the effective ink surface coverage a of the ink by minimizing the ΔE_{94} difference between the predicted reflectance and the measured reflectance:

$$\begin{aligned} a = \arg\min \big(\Delta E_{94} \big[&(1-a) R_{\text{Metal}}(\lambda) \\ &+ a T_{\text{Ink}}(\lambda)^2 R_{\text{Metal}}(\lambda),\ R_{\text{Measured}}(\lambda)\big]\big) \end{aligned} \tag{7}$$

where T_{Ink} is the transmittance of the ink layer, R_{Metal} is the reflectance of the metallic substrate and R_{Measured} is the measured reflectance of the line halftone. For obtaining effective surface coverages, the measurements are performed in the parallel mode, under specular reflection, at the (25°:25°) measurement geometry.

To establish the ink spreading curve, we first fit according to Eq. (7) the effective ink surface coverages for 25%, 50% and 75% of nominal ink surface coverages. We then establish the ink spreading curve by linear interpolation between the fitted effective ink surface coverages. Figure 7 shows the obtained ink spreading curves for each ink (cyan, magenta and yellow). The ink spreading curves are used to obtain the effective ink surface coverages from which the positions Ink_{Start} and Ink_{End} are calculated (Fig. 6).

5.4 *Full Algorithm*

Let us now present the steps for predicting the reflectance of the single colorant line halftone based on incident angle θ, the azimuthal rotation angle φ, the chosen ink, the ink surface coverage and the line screen frequency:

- Take the reflectance measurements of the fulltone inks (cyan, magenta and yellow) and approximate their transmittances with the formula

$$T_{\text{Ink}}(\lambda) = \sqrt{R_{\text{FulltoneInk}}(\lambda) / R_{\text{Metal}}(\lambda)} \tag{8}$$

where $T_{Ink}(\lambda)$ is the transmittance of the ink layer, $R_{\text{Metal}}(\lambda)$ is the reflectance of the metallic sheet and $R_{\text{FulltoneInk}}(\lambda)$ is the measured reflectance of the fulltone ink printed on the metallic sheet, all measured under specular reflectance at the (25°:25°) geometry.

Table I. For single colorant halftones, accuracy of the presented physical spectral prediction model expressed as average ΔE_{94} difference between predicted and measured reflectance spectra.

Accuracy of prediction model (mean ΔE_{94})	$\varphi = 90°$ (parallel mode)			$\varphi = 45°$			$\varphi = 0°$ (transverse mode)		
	50 lpi	100 lpi	150 lpi	50 lpi	100 lpi	150 lpi	50 lpi	100 lpi	150 lpi
$\theta = 25°$	2.4	3.9	4.8	2.7	3.8	4.5	3	4.5	5.4
$\theta = 45°$	2.5	3.7	4.6	3	4.8	4.9	3.7	5.1	4.2

- For each ink, deduce the ink spreading curve that accounts for the physical dot gain. These curves are established by applying formula (7) on the measurements taken with 25%, 50% and 75% nominal ink surface coverages in parallel mode. With the obtained effective ink surface coverages, define the Ink_{Start} and Ink_{End} positions.
- Using the incident angle θ, the azimuthal angle φ and the line screen frequency, we deduce the displacement value Δx with the following formulas:

$$\theta' = \arcsin\left(\frac{\sin(\theta)}{n'}\right) \tag{9}$$

$$\Delta x^{\circ} = \tan(\theta') \cdot d \tag{10}$$

$$\Delta x = \Delta x^{0^{\circ}} \cos(\varphi) \tag{11}$$

  where θ' is the incident angle inside the medium, n' is the refractive index of the transparent medium (we assume it is 1.5), $\Delta x^{0^{\circ}}$ is the displacement value calculated in meters for the line halftone observed in transverse mode ($\varphi = 0°$), d is the thickness of the polymer layer (here, $120 \cdot 0^{-6}$ m) and Δx is the displacement calculated for the azimuthal rotation angle of φ.
- Using the relative displacement value $\Delta x_{\text{norm}} = \Delta x / T$ and the effective surface coverages, we calculate the surface coverages of a_{imi}, a_{im}, a_{mi} and a_m with the algorithm presented in Section 5.2, formulas (2)–(6).
- Calculate the reflectance according to formula (1).

Note that the model is calibrated by measuring the reflectance of the bare metal layer and of the considered colorants with 25%, 50%, 75% and 100% surface coverages at the (25° : 25°) measuring geometry in parallel viewing mode. Therefore, in addition to the metal substrate reflectance, 4 calibration measurements per colorant are needed, i.e., a total of 25 measurements for the cyan, magenta, yellow, red, green and blue colorants for a specific line screen frequency.

5.5 *Prediction Accuracy*

We tested the presented physically based spectral prediction model on single colorant line halftones with different line frequencies (50, 100 and 150 lpi), different ink surface coverages (12.5%, 37.5%, 62.5% and 82.5%), different printed colorants (cyan, magenta, yellow, red, green and blue), different azimuthal rotation angles ($\varphi = 0°$, $\varphi = 45°$ and $\varphi = 90°$) and two incident angles, $\theta = 25°$ for the (25°:25°) and $\theta = 45°$ for the (45°:45°) measuring geometries. In total, our test set comprises $3 \cdot 4 \cdot 6 \cdot 3 \cdot 2 = 432$ measured halftones.

Table I describes the prediction accuracies expressed as CIELAB ΔE_{94} differences between the predicted color and the color of the sample measured under specular reflection.

The ΔE_{94} color differences are obtained by first converting reflectances to CIE-XYZ tristimulus values calculated with a D65 illuminant for the 2° standard observer. Then, the CIELAB color coordinates are calculated by using as white reference the spectral reflectance of the unprinted metallic substrate under the D65 illuminant [11].

From Table I we can conclude that the physical spectral prediction model is capable of predicting the spectral reflectance and the resulting color in function of the incident angle (θ), the azimuthal rotation angle (φ) and the screen frequency. We observe that when the sample is azimuthally rotated toward the transverse mode, the prediction accuracy tends to decrease.

When the azimuthal rotation angle is close to 0°, i.e., when the print is in transverse mode, the predicted reflectance relies mainly on the prediction of the *directional optical dot gain*. The approximate estimation of the *directional optical dot gain* according to Eqs. (3)–(6) seems to be the reason for this decrease in prediction accuracy.

Figure 8 shows a comparison between the predicted and the measured colors in the CIELAB lightness-chroma plane. The colors are compared for cyan halftones at 0%, 25%, 50%, 75% and 100% of surface coverage. The colors become more chromatic and darker when the line halftones are in transverse mode, with $\varphi = 0°$. We also considered two incident angles, (a) $\theta = 25°$ and (b) $\theta = 45°$. We observe that at angles further away from the normal ($\theta = 45°$), the *directional optical dot gain* is stronger, resulting in a more pronounced color change. Finally, we observe that the model is able to predict chroma and lightness of the line halftone as a function of the input incident (θ) and azimuthal (φ) angles.

6. PREDICTING LINE-ON-LINE INK HALFTONES

Let us extend the presented single colorant spectral prediction model to account for the line-on-line halftones printed with cyan, magenta and yellow ink. The colorants present in the halftone are formed by line-on-line superpositions of cyan, magenta and yellow halftones (Figure 9). Line-on-line

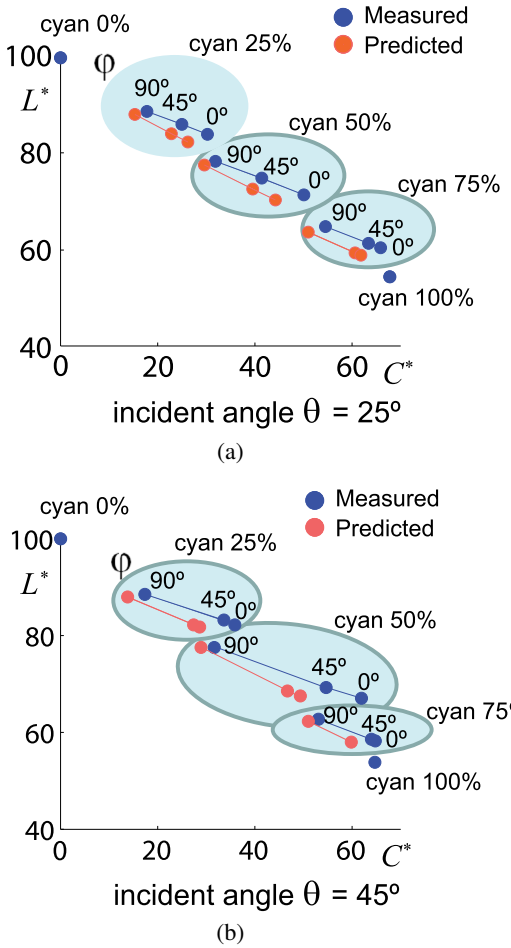

Figure 8. Illustration of the directional dot-gain effect by comparing the predicted and the measured colors in the lightness-chroma plane. The halftones are printed with cyan ink at 100 lpi. Selected surface coverages of cyan are 0%, 25%, 50%, 75% and 100%. The graphs show that when azimuthally rotating the line halftone print from $\varphi = 90°$ (parallel lines) to $\varphi = 0°$ (transversal lines), it becomes more chromatic and darker.

ink halftones behave similarly as the dot-on-dot halftones known from clustered dots screens [12].

$$a_k = c; \quad \text{surface coverage of the colorant black}$$
$$a_r = m - c; \quad \text{surface coverage of the colorant red}$$
$$a_y = y - m; \quad \text{surface coverage of the colorant yellow}$$
$$a_w = 1 - y; \quad \text{surface coverage of the colorant white}$$

We extend the concept of illuminant and observer projected areas (Fig. 3) to multiple colorants (Figure 10). Similarly, as in Section 5.2, for each of the printed colorant (U), we can calculate the projection areas A_{RI_U} and A_{IR_U} (Fig. 10). The A_{RI_U} projection area describes the area where light is reflected from the metallic layer and then passes through the colorant U. The A_{IR_U} projection area describes the area where light passes first through the colorant layer U and is then reflected from the metallic layer.

The a_{U1U2} areas (Figure 11) describe the space where the light passes through colorant $U1$, is reflected off the metallic layer and then passes through colorant $U2$. The

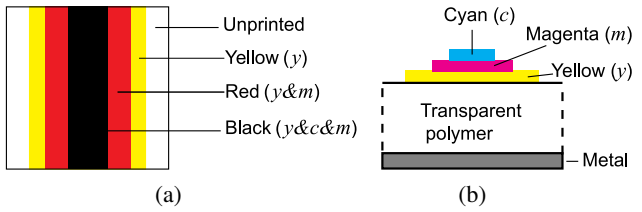

Figure 9. Graphical representation of a line-on-line printed *cyan*, *magenta*, *yellow* halftone, for $c \leq m \leq y$ where the & sign indicates the superposition of inks and c, m and y are ink surface coverages of *cyan*, *magenta* and *yellow*. The transparent polymer is located between the metallic layer and the ink halftone.

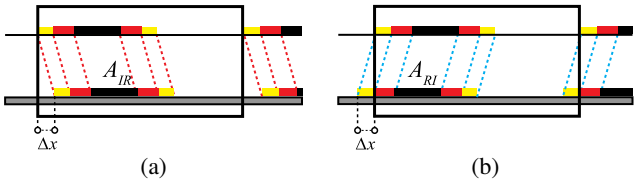

Figure 10. (a) Illuminant-based A_{IR} and (b) observer-based A_{RI} projections of the line halftones formed inside one screen element. The A_{IR} projection describes the area where light passes through the ink and is reflected by the metal. The A_{RI} projection describes the area where light is reflected off the metal and passes through the ink.

a_{U1U2} areas are formed by the intersecting $A_{IR\_U_1}$ and $A_{RI\_U_2}$ areas. Fig. 11 shows the illustration of all a_{U1U2} areas formed with the line halftone containing only yellow and red colorants. The two colorant halftones (red and yellow) are selected in order to simplify the illustration. In Figure 11, we observe that the a_{U1U2} area 3 is formed by the intersection of A_{IR_YELLOW} and A_{RI_RED} projections. The a_{U1U2} area 3 represents the space where light passes through the yellow ink, bounces off the metal and exits through the red colorant. Note that the red colorant is formed by the superposition of the magenta and yellow inks. Figure 12 shows the illustration of all a_{U1U2} areas when all three colorants are present in the line halftone (yellow, red and black). In this example, there is no intersection of A_{IR_BLACK} and A_{RI_BLACK} projections areas. This means that there is no area where light traverses the black colorant, reflects off the metal and then traverses again the black colorant. However, such an intersection area may occur when increasing the surface coverage of the black colorant or observing the halftone at a smaller angle with respect to the normal.

Once the transmittances of the colorants as well as the size of the corresponding a_{U1U2} areas are known, we can calculate the reflectance of the overall halftone with the following formula:

$$R(\lambda) = \sum_{U1,U2} a_{U1U2} T_{U1}(\lambda) R_{\text{Metal}}(\lambda) T_{U2}(\lambda) \qquad (12)$$

where $U1$ and $U2$ are the colorants present in the halftone, a_{U1U2} is the area where light passes through both $U1$ and $U2$, $T_{U1}(\lambda)$ and $T_{U2}(\lambda)$ are their transmittances and $R_{\text{Metal}}(\lambda)$ is the reflectance of the metallic layer. Note that Eq. (1) is a special case of Eq. (12), when only a single colorant is

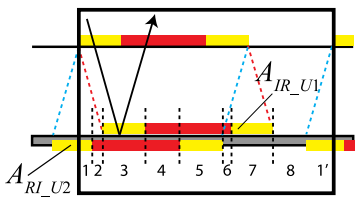

a_{U1U2}	A_{RI_U1}	A_{RI_U2}
1	no colorant	yellow
2	no colorant	red
3	yellow	red
4	red	red
5	red	yellow
6	red	no colorant
7	yellow	no colorant
8	no colorant	no colorant
1'	no colorant	yellow

Figure 11. Areas a_{U1U2} describing space where light passes through colorant $U1$, then reflects off the metal and then passes through colorant $U2$. The a_{U1U2} areas are calculated as intersections of all A_{IR_U1} and A_{RI_U2} areas. The line halftones are formed by yellow and red colorants, i.e., printed with yellow and magenta inks.

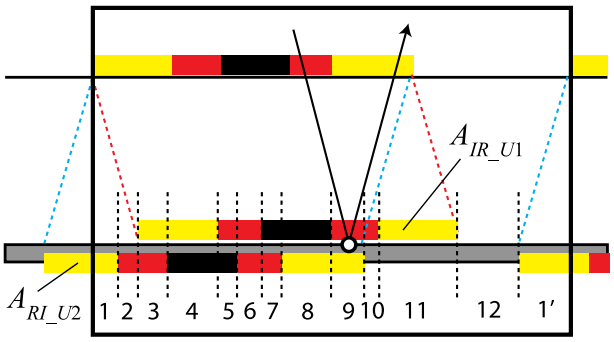

a_{U1U2}	A_{IR_U1}	A_{RI_U2}
1	no colorant	yellow
2	no colorant	red
3	yellow	red
4	yellow	black
5	red	black
6	red	red
7	black	red

a_{U1U2}	A_{IR_U1}	A_{RI_U2}
8	black	yellow
9	red	yellow
10	red	no colorant
11	yellow	no colorant
12	no colorant	no colorant
1'	no colorant	yellow

Figure 12. Areas a_{U1U2} with line halftones formed by yellow, red and black colorants, i.e., printed with yellow, magenta and cyan inks.

printed. If for certain A_{IR_U1} and A_{RI_U2} projection areas, there is no intersection area, the corresponding a_{U1U2} value is 0. For example, in Fig. 12, there is no intersection of the A_{IR_BLACK} and A_{RI_BLACK} projection areas.

To calculate the size of the a_{U1U2} areas, let us examine the cross-section of a line screen element (Fig. 10). In the same manner as in Section 5.2, the projection areas A_{RI_U} and A_{IR_U} are wrapped within one tile. To calculate A_{RI_U} and A_{IR_U}, we first have to determine the colorant's (U) position within the screen element (Figure 13). The position and the size of the colorants within the screen element can be calculated if the line center (in Fig. 13, the line center is at the center of ink_1) and all printed ink surface coverages (ink_1, ink_2 and ink_3) are known. We describe the position and the size of the central colorant (black, Fig. 13) with two points [$Colorant_{\text{Start}}$, $Colorant_{\text{End}}$]. In case of other colorants (red and yellow, Fig. 13), we use four points [$ColorantLeft_{\text{Start}}$, $ColorantLeft_{\text{End}}$] and [$ColorantRight_{\text{Start}}$, $ColorantRight_{\text{End}}$]. Once the position of each colorant is determined, we use the algorithm presented in Section 5.2 and Eqs. (2) and (5) to determine the A_{RI_U} and A_{IR_U} projections, for each colorant U, within the screen element (insert $Ink_{\text{Start}} = Colorant_{\text{Start}}$ and $Ink_{\text{End}} = Colorant_{\text{End}}$ in Eq. (3)). If the colorant is split onto the left and the right parts (red and yellow, Fig. 13), we apply Eqs. (2)–(5) separately to both parts, [$ColorantLeft_{\text{Start}}$, $ColorantLeft_{\text{End}}$] and [$ColorantRight_{\text{Start}}$, $ColorantRight_{\text{End}}$]. The detailed algorithm yielding the position and the size of the colorants within the screen element is presented in Section 6.1.

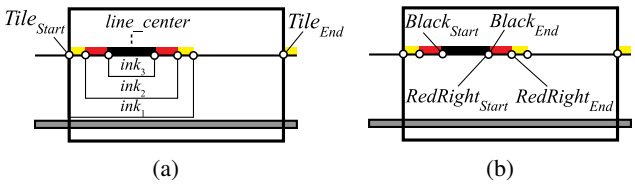

Figure 13. The position and the size of each colorant can be calculated with the ink surface coverages of ink_1 (yellow), ink_2 (magenta) and ink_3 (cyan).

6.1 *The Line-on-line Halftone Prediction Algorithm*

Let us now present the algorithm for calculating the reflectance of the line-on-line halftone based on the incident angle θ, the azimuthal rotation angle φ, the ink surface coverages and the line screen frequency:

- Take the reflectance measurements of the fulltone colorants (cyan, magenta, yellow, red, green, blue and black) and approximate their transmittances with formula (8).
- For each ink (cyan, magenta and yellow), deduce in parallel mode, i.e., with halftone lines parallel to the incoming light, the ink spreading curve that accounts for the physical dot gain. These curves are established by applying formula (7) on the measurements taken with 25%, 50% and 75% nominal ink surface coverages. The effective surface coverage obtained from the mapping between nominal to effective surface coverages defined by the ink spreading curve defines the ink start and end positions of each ink.
- According to Eqs. (9) and (11), with incident angle θ, azimuthal angle φ and the line screen frequency, deduce the displacement value Δx as well as the normalized displacement value $\Delta x_{\text{norm}} = \Delta x / T$.
- Determine the order of surface coverages of printed cyan, magenta and yellow ink halftones, i.e., find $ink_1 > ink_2 > ink_3$.
- Find the center of the printed line halftone $line\_center = ink_1/2$ (Fig. 13).
- Calculate the colorant size and positions inside the screen element:

Area covered with superposition of ink_1, ink_2 and ink_3 (Fig. 13, black colorant):

$-[line\_center - ink_3/2,\ line\_center + ink_3/2] : center\ of\ the\ halftone.$

Area covered with superposition of ink_1, ink_2 (Fig. 13, red colorant):

$-[line\_center - ink_2/2,\ line\_center - ink_3/2] : left\ from\ ink_3$

$-[line\_center + ink_3/2,\ line\_center + ink_2/2] : right\ from\ ink_3$

Area covered with ink_1 (Fig. 13, yellow colorant):

$-[line\_center - ink_1/2,\ line\_center - ink_2/2] : left\ from\ ink_2$

$-[line\_center + ink_2/2,\ line\_center + ink_1/2] : right\ from\ ink_2.$

Area not covered with any ink (Fig. 13, no colorant):
$-[line\_center + ink_1/2, Tile_{\mathrm{End}}] : right\ from\ ink_1$

- For each of the colorant areas deduced in the previous step, calculate the projections A_{RI_U2} and A_{IR_U1} inside the screen tile with Eqs. (2) and (5), where U is the colorant present in the line halftone.
- Then for all combinations of colorants $U1$ and $U2$, calculate a_{U1U2} as intersection of A_{RI_U2} and A_{IR_U1} ($a_{U1U2} = A_{RI\_U2} \cap A_{IR\_U1}$). If for certain A_{IR_U1} and A_{RI_U2} projection areas there is no such intersection, set $a_{U1U2} = 0$.
- Finally, with formula (12), calculate the reflectance of the overall halftone.

Note that the multi-ink halftone prediction model is calibrated by measuring the reflection spectra of the bare metal and of all seven fulltone colorants at the (25° : 25°) measurement geometry as well as the cyan, magenta and yellow inks at 25%, 50% and 75% nominal halftone surface coverages, i.e., a total of $8 + 9 = 17$ measurements for a specific line screen frequency.

6.2 *Prediction Accuracy*

We tested the presented physically based spectral prediction model on the line halftones formed by all combinations of ink surface coverages (cyan, magenta and yellow) of 0%, 25%, 50%, 75% and 100%, different azimuthal rotation angles ($\varphi = 0°$, $\varphi = 45°$ and $\varphi = 90°$) and two incident angles ($\theta = 25°$ and $\theta = 45°$). The line halftones are printed at 100 lpi. In total, our test set comprises 750 measured halftones. Table II gives the prediction accuracy.

From Table II, we conclude that the physical spectral prediction model is capable of predicting the spectral reflectance of halftones at a screen frequency of 100 lpi in function of the incident angle (θ) and the azimuthal rotation angle (Φ). We observe that the prediction accuracy is slightly worse compared with the predictions of single colorant lines (Section 5.5, Table I). We observe that when the sample is viewed under large incident angles ($\theta = 45°$) or when the sample is rotated (lines are transversal to the incident light, $\Phi = 0°$), the prediction accuracy decreases.

Table II. Accuracy of the presented physical spectral prediction model expressed as average ΔE_{94} difference between predicted and measured reflectance spectra, under specular viewing conditions.

Prediction accuracy (mean ΔE_{94} at 100 lpi)	$\varphi = 90°$ (parallel mode)	$\varphi = 45°$	$\varphi = 0°$ (transversal mode)
$\theta = 25°$	3.4	4.9	5.9
$\theta = 45°$	4.3	6.6	7

Figure 14 shows a comparison between the predicted and the measured colors in the chromaticity plane (CIELAB a^*b^* plane). We selected halftones that have high chroma values formed with ink surface coverages of 0%, 25% and 50%. Colors are more chromatic when the sample is shown in transverse mode ($\varphi = 0°$). We observe that the predicted colors are less chromatic than the measured colors. This may be due to multiple internal reflections occurring between the print–air interface and the metallic layer, which are not accounted for in the present model. We also observe that there are some deviations in the prediction of the hue. This may be due to the simple light traversal assumption used for the deduction of the transmittance of the ink layer according to Eq. (8). Nevertheless, from Fig. 14 and Table II, we conclude that we correctly predicted the color of the line-on-line halftones under specular reflection at freely chosen azimuthal rotation and incident viewing angles.

7. CONCRETE EXAMPLE

As a concrete example benefiting from the color changing capabilities of the line halftone upon azimuthal rotation of the sample, we have realized a security label whose colors change strongly upon azimuthal rotation of the sample (Figure 15). The sample is realized with superposed greenish horizontal halftone lines and reddish vertical halftone lines within the cross and in the background of the label (areas A). The background of the Swiss flag contains superposed reddish horizontal halftone lines and greenish vertical halftone lines (area B).

When the sample is laid out horizontally (Fig. 15a), light from a window located opposite to the camera illuminates in area A the horizontal greenish lines which induce a large dot gain and the vertical reddish lines which induce a negligible dot gain. The resulting color of areas A is therefore greenish. In area B, similar considerations apply, but the greenish and reddish halftone lines are exchanged and this area looks, therefore, lavender-reddish. When the sample is rotated by 90° (Fig. 15b), the previously horizontal halftone lines become vertical with a low dot gain and the previously vertical halftone lines become horizontal with a strong dot gain. The corresponding colors are therefore inverted.

8. CONCLUSIONS

We presented a physically based spectral prediction model that predicts the color in specular viewing mode in function

Ink surface coverages

	(c, m, y)						
1	(0, 0, 0.5)	4	(0, 0.5, 0.25)	7	(0.5, 0.5, 0)	10	(0.5, 0, 0.25)
2	(0, 0.25, 0.5)	5	(0, 0.5, 0)	8	(0.5, 0.25, 0)	11	(0.5, 0, 0.5)
3	(0, 0.5, 0.5)	6	(0.25, 0.5, 0)	9	(0.5, 0, 0)	12	(0.25, 0, 0.5)

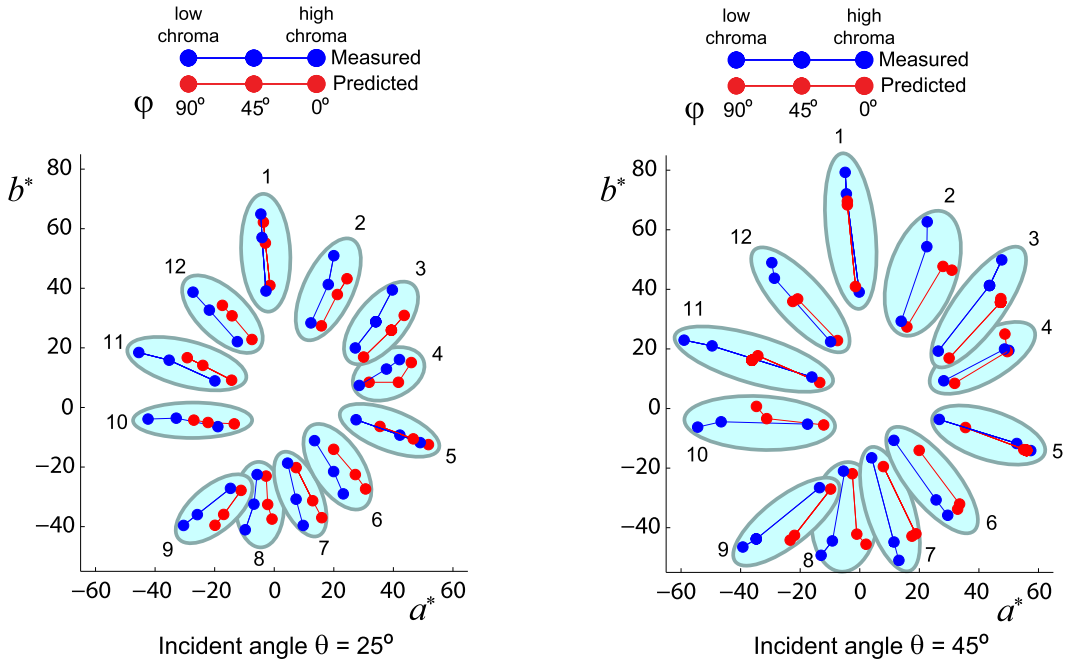

(a) (b)

Figure 14. Comparison between predicted and measured colors in the chromaticity plane (CIELAB a^*b^* plane) and directional dot-gain effect for halftones having high chroma values (ink surface coverages of 0%, 25% and 50%). When azimuthally rotating the halftones from $\varphi = 90°$ (parallel mode) to $\varphi = 0°$ (transversal mode), they become more chromatic. At larger incident angles, the directional optical dot gain is stronger.

(a) (b)

Figure 15. Photographs of the same sample at the two azimuthal orientations 0° and 90°, illuminated from a window located opposite to the camera and above the sample (courtesy: Usines Métallurgiques de Vallorbe).

of line-on-line ink surface coverages, the incident angle θ, the azimuthal rotation angle φ and the line screen frequency f_l. We model the interaction of the light and the print medium incorporating a metallic substrate. Because of the thickness of the ink-receiving transparent polymer layer, under specular reflection and in transverse orientation, the effective area from which the light is reflected (a_m) without traversing the ink layer is reduced (Fig. 2). The size of the printed halftone is optically increased, thereby producing darker and more chromatic colors. This effect is called *directional optical dot gain*. Furthermore, because of the metal layer, which does not diffuse light, the intensity of this effect depends on the halftone shape and its azimuthal orientation. The line halftones exhibit the strongest color change upon azimuthal rotation by 90°.

The presented algorithm calculates the apparent surface coverages of the colorants by accounting for the *directional optical dot gain*. It relies on the projected halftone areas along the illumination and observation directions. The model also accounts for Snell's refraction of light into the print medium. Finally, the model accounts for the physical dot gain of the inks by fitting the ink surface coverages in parallel mode, i.e., when the line halftone has the same orientation as the incident specularly reflected light that reaches the observer.

We have extended the single colorant model to account for line-on-line halftones viewed under specular observation conditions. The multi-ink color prediction model predicts the color of the cyan, magenta and yellow line halftones as a function of the azimuthal angle of the print, the incident angle of light and the surface coverages of the inks. The

prediction accuracy is comparable to the one of the single colorant model.

As future work, one may try to improve the accuracy of the prediction model by accounting for the Fresnel reflection at the air–print interface and the multiple internal Fresnel reflections between the metallic surface and the print–air interface.

ACKNOWLEDGMENT

We thank Sergio Lizzola for having created a joined project among Innoview Sàrl (Dr Romain Rossier), EPFL (Dr P. Pjanic, Prof. R. D. Hersch) and Usines Métallurgiques de Vallorbe (François Galloppini) that aimed at designing security labels based on the know-how related to the present publication and to prior research [8].

REFERENCES

[1] R. D. Hersch, F. Collaud, and P. Emmel, "Reproducing color images with embedded metallic patterns," ACM Trans. Graph. **22**, 427–436 (2003).

[2] W. Matusik, B. Ajdin, J. Gu, J. Lawrence, H. P. A. Lensch, F. Pellacini, and S. Rusinkiewicz, "Printing spatially-varying reflectance," ACM Trans. Graph. **28**, 9 (2009).

[3] T. Malzbender, R. Samadani, S. Scher, A. Crume, D. Dunn, and J. Davis, "Printing reflectance functions," ACM Trans. Graph. **31**, 11 (2012).

[4] V. Babaei and R. D. Hersch, "Yule-Nielsen based multi-angle reflectance prediction of metallic halftones," SPIE **9395**, 10 (2015).

[5] V. Babaei and R. D. Hersch, "Color reproduction of metallic-ink images," J. Imaging Sci. Technol. **60**, 10 (2016).

[6] P. Pjanic and R. D. Hersch, "Specular color imaging on a metallic substrate," *Proc. IS&T CIC21: Twenty-First Color and Imaging Conf.* (IS&T, Springfield, VA, 2013), pp. 61–68.

[7] P. Pjanic and R. D. Hersch, "Color imaging and pattern hiding on a metallic substrate," ACM Trans. Graph. **34** 10 (2015).

[8] P. Pjanic and R. D. Hersch, "Color changing effects with anisotropic halftone prints on metal," ACM Trans. Graph. **34**, 12 (2015).

[9] H. E. J. Neugebauer, "Die theoretischen Grundlagen des Mehrfarbendrucks," *Zeitschrift fuer wissenschaftliche Photographie* (1937), Vol. 36, pp. 36–73, translated by D. Wyble and A. Kraushaar, in "The theoretical basis of multicolor letterpress printing," Color Res. Appl. **30**, 322–331 (2005).

[10] R. D. Hersch and F. Crété, "Improving the Yule-Nielsen modified spectral Neugebauer model by dot surface coverages depending on the ink superposition conditions," SPIE **5667**, 434–445 (2005).

[11] G. Sharma, "Color fundamentals for digital imaging," in *Digital Color Imaging Handbook*, edited by G. Sharma (CRC Press, Boca Raton, Florida, 2003), pp. 1–40.

[12] R. Balasubramanian, "A printer model for dot-on-dot halftone screens," SPIE **2413**, 356–364 (1995).